JOURNAL OF GEOPHYSICAL RESEARCH, VOL. 102, NO. C2, PAGES 3421–3438, FEBRUARY 15, 1997

Increased coastal upwelling in the California Current System

Franklin B. Schwing and Roy Mendelssohn

Pacific Fisheries Environmental Group, Pacific Grove, California

Abstract. State-space statistical models are applied to long environmental time series of monthly northward wind stress, sea surface temperature (SST), salinity (SSS), and sea level (SL) from the west coast of North America. The models use a combination of Kalman filtering and maximum likelihood methods, which estimate a nonlinear trend, a nonstationary and nondeterministic seasonal signal, and an autoregressive term, and effectively separate the seasonal signals from the long-term trends. The seasonal series are examined for behavior consistent with increasing coastal upwelling during the spring–summer upwelling "season," presumably in response to a pattern of long-term global warming. Over a region of the California Current System (CCS) where coastal upwelling is a dominant process (32–40°N), wind stress, SST, SSS, and SL all show strong evidence of a systematic intensification of upwelling during April–July. Model trend series suggest a linear tendency for increasing equatorward stress (in agreement with the seasonal tendency), but warmer SST (opposite the seasonal and the expectation of greater upwelling). The linear tendencies of the SST and stress trends are generally an order of magnitude greater than the seasonal tendencies. Thus the long-term trend in SST masks the cooling effect of increased seasonal upwelling, and the trend in equatorward stress suggests an artificially large seasonal increase in the observed spring and summer stress. A key to identifying these patterns has been the ability to separate the long- term nonlinear trend, using the state-space models, which mask the signal of increased upwelling in the observations.

1. Introduction

Climate variability on very large time scales (century) and space scales (global) impacts, or has the potential to impact, marine ecosystems at a variety of smaller scales. A number of recent papers have explored the patterns and dynamics of fluctuations embedded within the long-term, globally integrated tendency commonly referred to as climate change ([*Trenberth,* 1990; *Mann and Park,* 1993, 1994, 1996; *Graham,* 1994; *Latif and Barnett,* 1994; *Miller et al.,* 1994; *Trenberth and Hurrell,* 1994; *Ware,* 1995] to name but a few). However, these studies have concentrated on large-scale temporal oscillations, generally on decadal scales; fewer examples [cf. *Parrish et al.,* 1981] describe variability on subbasin (i.e., 100–1000 km) space scales.

In a particularly striking example of how global climate change may be affecting ocean conditions on smaller scales, *Bakun* [1990] postulates that under the scenario of global warming, continental air masses will warm more rapidly than oceanic air masses, leading to an intensified summer continental atmospheric low, a greater cross-margin pressure gradient between the continental low and higher pressure over the cooler ocean, stronger equatorward wind stress, and increased coastal upwelling along eastern ocean boundaries. The effect on eastern boundary current (EBC) systems could be significant because of the highly productive nature of these ecosystems and their potentially important role in the global CO_2 budget.

Upwelling is not a temporally continuous or spatially uniform process, but displays periods of upwelling and downwelling favorable conditions (as well as substantial interannual variability) and has a distribution that suggests certain regions or sites are more conducive to upwelling [*Rosenfeld et al.,* 1994]. Empirical studies of upwelling and its effects on biological production suggest that optimal fisheries production in EBCs occurs within a limited range of wind speeds; at speeds greater than about 5–7 m/s the biomass of small pelagic fish decreases [*Cury and Roy,* 1989]. This has resulted in ecosystems that are tuned to these variations. Any long-term changes in the seasonal patterns of upwelling, their intensity or the duration of upwelling events could have dramatic implications to EBC ecosystems and their living marine resources.

Because upwelling has a very complex and regionalized spatial structure, its character cannot be determined or quantified with spatially integrated indices

Paper number 96JC03591.

(e.g., globally or ocean-averaged sea surface temperature (SST) time series), or with a single index from an isolated location. For example, *Mann and Park* [1993] show that interdecadal atmospheric temperature signals exhibit spatial variability that leads to considerable cancellation in a global average. *Ware* [1995] suggests that fluctuations in northeast Pacific coastal temperature on four subcentury scales moderate long-term climate trends. Analogously, because of its seasonal nature, annual averages or low-pass "smoothed" time series will not reveal potential changes in upwelling. Monthly averaged time series include the upwelling signal, but temporal changes in upwelling on decadal to century scales could be concealed by long-term trends related to other factors (i.e., cooler SST in spring-summer due to increased upwelling may be masked by a general warming pattern).

In this paper, we take advantage of a unique set of multidecadal coastal environmental data from along the west coast of North America and introduce existing statistical modeling techniques to the area of climate research, to evaluate changes in the seasonal nature of EBC atmospheric forcing and the oceanic response. In particular, we test the hypothesis of *Bakun* [1990] that equatorward wind stress in spring and summer, hence coastal upwelling, has been increasing in EBCs over the past several decades, presumably in response to a long-term global warming trend. We apply state-space models [cf. *Shumway,* 1988, chap. 3; *Harvey,* 1989] to separate the seasonal component from the long-term trend in a variety of California Current System (CCS) environmental time series, and examine the variability in the seasonal component on climate (decadal and longer) scales. We emphasize that our focus is on long-term changes in the seasonal cycle. These are separate and independent from the series' trends produced by the statistical model, which contain the patterns and variations described by *Trenberth* [1990], *Graham* [1994], *Latif and Barnett* [1994], *Miller et al.* [1994], *Trenberth and Hurrell* [1994], and others, and are presented separately [*Schwing et al.,* 1997].

2. Methods

2.1. Time Series

The monthly averaged time series described here were generated from a variety of sources. The primary database was the Comprehensive Ocean-Atmosphere Data Set (COADS). The COADS contains almost 100 million reports of ocean surface conditions, mostly taken by ships-of-opportunity. The data have been collected, quality-controlled and put into common formats and units [*Slutz et al.,* 1985; *Woodruff et al.,* 1987]. Data were extracted using the CD–ROM-based version of COADS and the CODE extraction program described by *Mendelssohn and Roy* [1996]. The CD–ROM version contains Release 1 of COADS for the period 1854–1979 and the Interim release for 1980–1990, in CMR5 format. The wind data are marked as estimated, for winds approximated using the Beaufort scale; as measured, for anemometer or buoy measurements; or as unknown, when the measurement method and device were not known. Only wind data marked as estimated or unknown were used in forming the mean series, to avoid as much as possible the known bias in the data due to an increase over time in the use of anemometers to mea-

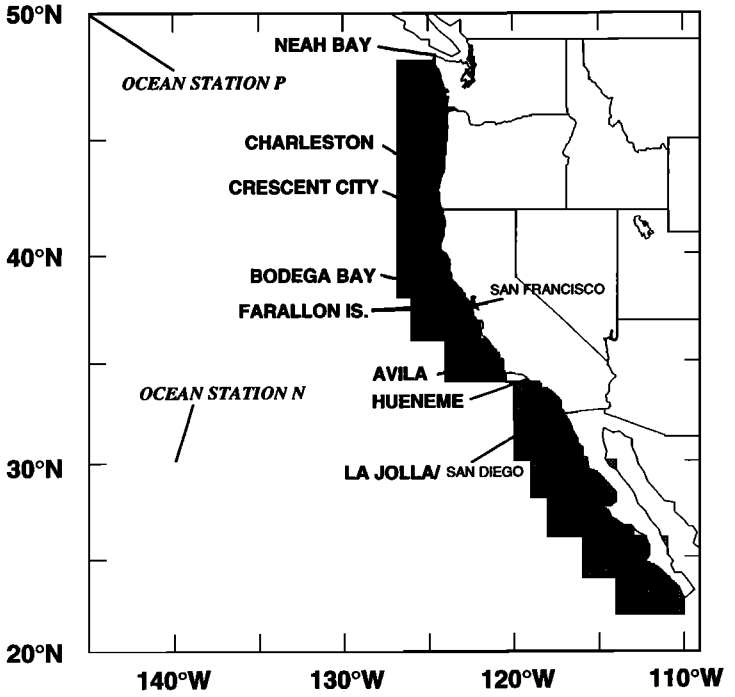

Figure 1. Locations of COADS 2° boxes, shown as shaded boxes, and coastal stations from which monthly time series were generated. Locations of Ocean Stations P and N are also shown.

Table 1. Dimensions of COADS Boxes Containing Derived Monthly Averaged Equatorward Wind Stress and SST (for Period 1946-1990), and Selected Shore Stations Adjacent to the COADS Boxes

COADS Box	COADS Latitude	COADS Longitude	Shore Station	SST	SSS	SL
47N	46-48°N	124-127°W	Neah Bay (48°22')	1935-92	1936-92	1934-92
45N	44-46°N	123.5-127°W				
43N	42-44°N	124-127°W	Charleston (43°21')	1966-92		
41N	40-42°N	123-127°W	Crescent City (41°45')	1933-92	1934-92	1933-92
39N	38-40°N	122-127°W	Bodega Bay (38°19')	1957-92	1975-92	
37N	36-38°N	122-126°W	Farallon (37°42')	1925-92	1925-92	1915-92
35N	34-36°N	120.5-124°W	Avila (35°10')	1945-92	1945-79	
Bight	32-34°N	116-120°W	Hueneme (34°09')	1919-87	1919-63	
			La Jolla (32°52')	1916-92	1926-92	1915-92
31N	30-32°N	116-120°W				
29N	28-30°N	114-119°W				
27N	26-28°N	113-118°W				
25N	24-26°N	111-116°W				
23N	22-24°N	110-114°W				
			Ocean Station P (50°N,145°W)	1950-92	1956-92	
			Ocean Station N (30°N,140°W)	1954-74		

Dates for monthly averaged time series of coastal SST, coastal salinity (SSS) and sea level (SL). SL measured at San Francisco and San Diego are used for Farallon and La Jolla, respectively.

sure the wind [*Cardone et al.*, 1990; *Isemer*, 1992; *Wu and Newell*, 1992]. Based on statistics from the data set, each observation for each parameter has been flagged as to the "quality" of the observation [see *Slutz et al.*, 1985, page D6]. Poleward (northward) pseudostress, henceforth referred to as wind stress, was derived by squaring the northward wind component from each record extracted prior to monthly averaging. Spatial regions approximately 2° latitude by 4° longitude were defined based on a combination of ecological and oceanographic features as well as data density, and time series of poleward wind stress and SST were calculated for each region (Figure 1, Table 1) from the monthly means of each variable. To exclude possibly erroneous observations, all COADS data outside of their "wide interval" (roughly equal to three standard deviations) were excluded from the averaging. These geographic boxes are referred to in terms of their central latitude (e.g., 23N refers to the 22–24°N COADS box). The time period of extraction is 1946–1990.

Shore-based monthly SST and salinity (SSS) time series were averaged from daily observations made by volunteers, which were sent to the Marine Life Research Group, Scripps Institution of Oceanography [cf. *Walker et al.*, 1993]. SSTs were reported to the nearest 0.1°C at most sites. The observations are accurate to about ±0.2°C. Salinities were determined at Scripps from daily seawater samples using an inductive salinometer. Daily observations were quality controlled prior to the monthly averaging. The number of daily values varied from 15 to 20 per month (and as few as 10 per month during winter months) at some of the northern stations (e.g., Farallon, Crescent City), to nearly complete coverage (e.g., La Jolla). Since 1979, NOAA/National Ocean Service (NOS) has measured density with a hydrometer at Neah Bay and Crescent City. Salinities were back-calculated from these monthly averaged densities. The locations of shore stations are shown in Figure 1 and Table 1.

Monthly averaged time series of sea level (SL) were supplied by NOAA/NOS, some through the Pacific Climate (PACLIM) database [*Cayan et al.*, 1988]. Long SL series are available at four sites (Figure 1, Table 1). With a few exceptions, missing values in the shore time series were sparse and of only 1 to a few months' duration. The time and space averaging for the COADS series was selected to ensure no missing observations while maximizing resolution. Months with no data were included in the analysis; the model fits through periods of missing data.

2.2. State-Space Statistical Model

To estimate a time-varying (i.e., nonstationary) seasonal component for each time series, we assume that each observation $y(t)$ is the sum of four components:

$$y(t) = T(t) + S(t) + I(t) + e(t) \qquad t = 1, T \qquad (1)$$

where, at time t, $T(t)$ is the unobserved time-dependent mean-level (trend), $S(t)$ is the seasonal component, $I(t)$ is the irregular term (stationary but autocorrelated), and $e(t)$ is the stationary uncorrelated component which can be viewed here as "observation" or "measurement" error.

The model (equation (1)) must be more fully specified to be meaningful. The use of piecewise continuous "smoothing splines" to estimate the unobserved components dates back to *Thiele* [1880] [see *Lauritzen*, 1981]

and, in the more modern era, to a paper by *Whittaker* [1923]. Lauritzen provides an excellent summary of how more modern state-space models relate to these pioneering works.) *Shiller* [1973] modeled a distributed lag (impulse response) relationship between the input and output of time series under difference equation "smoothness" constraints on the distributed lags. He termed these constraints "smoothness priors" but did not offer an objective method of choosing the smoothing parameter. *Akaike* [1980] developed a Bayesian interpretation of the model and used maximum likelihood methods to estimate the smoothness parameter. *Brotherton and Gersch* [1981] showed how the Kalman filter and maximum likelihood could be used to solve the smoothing problem, which was the first attempt to our knowledge to combine the techniques applied here. *Kitagawa and Gersch* [1984, 1985, 1988], in a series of papers, used smoothness priors to model a variety of nonstationary problems, and *Harvey* [1989] developed similar models under the title "structural time series models."

The methodology can be most clearly understood in terms of estimating a "smooth" but unknown function which has been observed with "noise," that is, data of the form

$$y(t) = f(t) + e(t) \tag{2}$$

where the $y(t)$ are the observed data, $f(t)$ is an unknown smooth function, and $e(t)$ are independent Gaussian errors. *Whittaker* [1923] suggested that the solution should balance fidelity to the data with fidelity to a smoothness constraint:

$$\left[\sum_{t=1}^{T}(y(t) - f(t))^2 + \mu^2 \sum_{t=1}^{T}(\nabla^k f(t))^2\right]. \tag{3}$$

The first term in equation (3) is the usual sum-of-squares criterion, while the second term constrains the kth-order finite differences of the unknown function, the discrete equivalent of splines where the kth-order derivatives are constrained. The two parts are balanced by the smoothness parameter μ. (Equation (3) is equivalent to a Lagrangian multiplier formulation of a sum-of-squares problem constrained by the kth-order differences set equal to zero.) As $\mu \rightarrow 0$, the smoothness constraint becomes negligible, and the solution exactly interpolates the data. As $\mu \rightarrow \infty$, the sum-of-squares term becomes negligible, and the solution is the appropriate kth-order polynomial (linear for $k = 1$, quadratic for $k = 2$, etc.)

Akaike [1980] gave the problem a Bayesian interpretation, where the smoothness constraint is viewed as a stochastic perturbed, zero-mean difference equation,

$$\nabla^k f(t) \sim N(0, \sigma^2) \tag{4}$$

where $\mu^2 = \frac{1}{\sigma^2}$, which can be interpreted as a signal-to-noise ratio, is a hyperparameter that can be estimated using maximum likelihood methods. *Ansley and Kohn* [1986] and *Kohn and Ansley* [1988] have shown that for a diffuse initial prior (that is, when it is assumed there is no prior information about the state vector at time zero), the solution produced by this problem is the discrete equivalent of the smoothing spline discussed extensively by Wahba and co-workers for nonparametric function estimation [see *Wahba*, 1990 and references therein], except that the smoothness parameter is estimated by maximum likelihood instead of generalized cross-validation (see *Wahba* [1990] for a discussion of generalized cross-validation; see also *Wecker and Ansley* [1983]).

Returning to equation (1), the trend term can be viewed as an unknown function of time, and parameterized as

$$\nabla^k T(t) \sim N(0, \sigma_T^2). \tag{5}$$

The seasonal component can be constrained in several fashions. In the first, the running sum of the seasonal component is constrained (assuming s periods in a season; e.g., $s = 12$ for monthly data, $s = 4$ for quarterly data):

$$\sum_{i=0}^{s-1} S(t-i) \sim N(0, \sigma_S^2) \qquad t = 1, T. \tag{6}$$

A second approach constrains the seasonal differences:

$$S(t) - S(t-s) \sim N(0, \sigma_S^2) \qquad t = 1, T. \tag{7}$$

Another approach is to model the seasonal component using a second-order autoregressive (AR(2)) term, with the autoregressive parameters fixed but the innovation variance (i.e., σ_S^2 in equations (6) and (7)) to be estimated. The proper choice of the AR(2) parameters will create a component at a given frequency but with a changing phase and amplitude. *Harvey* [1989] describes a related approach using trigonometric functions. In this paper, we use the first approach, as it would appear to provide the most flexibility in describing a seasonal component that could be a sum of annual and higher frequencies, as some of the time series suggest. Alternative methods for estimating the seasonal cycle in time series nonparametrically [e.g., *Rajagopalan and Lall*, 1995; *Thomson*, 1995] or using multivariate complex demodulation methods [*Mann and Park*, 1996] could be applied to this problem.

The irregular term $I(t)$ is assumed to be a pth-order autoregression, that is,

$$I(t) = \sum_{i=1}^{p} \phi_i I(t-p) + \epsilon(t); \tag{8}$$

$$\epsilon(t) \sim N(0, \sigma_I^2) \qquad t = 1, T \tag{9}$$

and the observation errors are assumed to be zero mean, independent, and identically distributed as

$$e(t) \sim N(0, \sigma_e^2) \qquad t = 1, T. \tag{10}$$

Kitagawa and Gersch [1984, 1988] show how these assumptions can be put into a state-space model and solved by using a combination of the Kalman filter and maximum likelihood. *Shumway and Stoffer* [1982] and *Shumway* [1988, chap. 3] show how the expectation-maximization (EM) algorithm [*Dempster et al.*, 1977] can be used to calculate the maximum likelihood estimates. The minimum mean-squared error estimates

of each of the components are given by the Kalman smoother calculated at the final maximum likelihood estimates of the hyperparameters.

Details of the likelihood equations and the necessary computations are given in the appendix. The appropriateness of this method and the constraints applied are discussed in the references [cf. *Kitagawa and Gersch*, 1984, 1985, 1988; *Young et al.*, 1991). A similar model was used by *Young et al.* [1991] to model the Mauna Loa atmospheric CO_2 time series and a time series composed of the first principal component of Pacific Ocean SST anomalies. *Rajagopalan and Lall* [1995] use a similar method, with a different choice of smoother, to describe phase shifts in the seasonal cycle of precipitation in the western United States. To our knowledge, however, this is the first use of these state-space methods to interpret geophysical or environmental data.

In all of our analyses, we use $k = 1$ in the trend (equation (5)), so that the first-order differences are assumed to be random, $p = 1$ in equation (9) for a first-order autoregressive (AR(1)) term, and the seasonal prior term given in equation (6) with $s = 12$, as we are analyzing monthly data. Sensitivity studies using a second-order autoregressive irregular term show the trend and seasonal components to be essentially identical to those with the AR(1), and that the AR(2) term is dominated by the AR(1) term. We also examined various subsets of the data and found the results of the algorithm are not affected by truncating the series; i.e., the trend and seasonal components are virtually unchanged.

The flexibility of this parameterization can be understood best by examining the limits of the trend and seasonal components at the extremes of their variances when the other components have been removed (the partial residual series). If the seasonal and irregular terms were somehow known, then the algorithm would estimate a smoothed version of the observed series minus the seasonal and irregular components, in this case the discrete equivalent of a kth-order smoothing spline. When the trend variance (σ_T^2) is zero, this smoother is simply a linear least squares fit to the partial residual series. As $\sigma_T^2 \rightarrow \infty$, the smoother interpolates the partial residual series.

If the trend and irregular were removed from the data, then the algorithm calculates for the seasonal component given by equation (6), a smoothed version of the s-period running sums of the partial residual series, where the amount of smoothing applied is the same throughout the series. This implicitly will smooth the s-period differences also. When the seasonal variance (σ_S^2) is zero, the result is the monthly means of the partial residual series. As $\sigma_S^2 \rightarrow \infty$, the result again interpolates the partial residual series.

Likewise, if the trend and seasonal components were known, then the irregular term estimates a pth-order autoregressive model of the partial residual series with the trend and the seasonal removed. While the algorithm used in this paper estimates the components simultaneously, this "backfitting" type approach of recursively smoothing the partial residual series could be used with other smoothing algorithms.

This process of smoothing the partial residual given the other components can be understood more clearly by examining some of the 37N (36–38°N) COADS time series. A well-defined annual SST cycle is superimposed on the nonlinear model trend (Figure 2a). The estimated trend is apparent when the seasonal component is removed (Figure 2b). When the trend is removed from the data, the partial residual series has zero mean as desired, but compared to the estimated seasonal component, some autocorrelation remains (difference between black and gray lines in Figure 2c). When both the

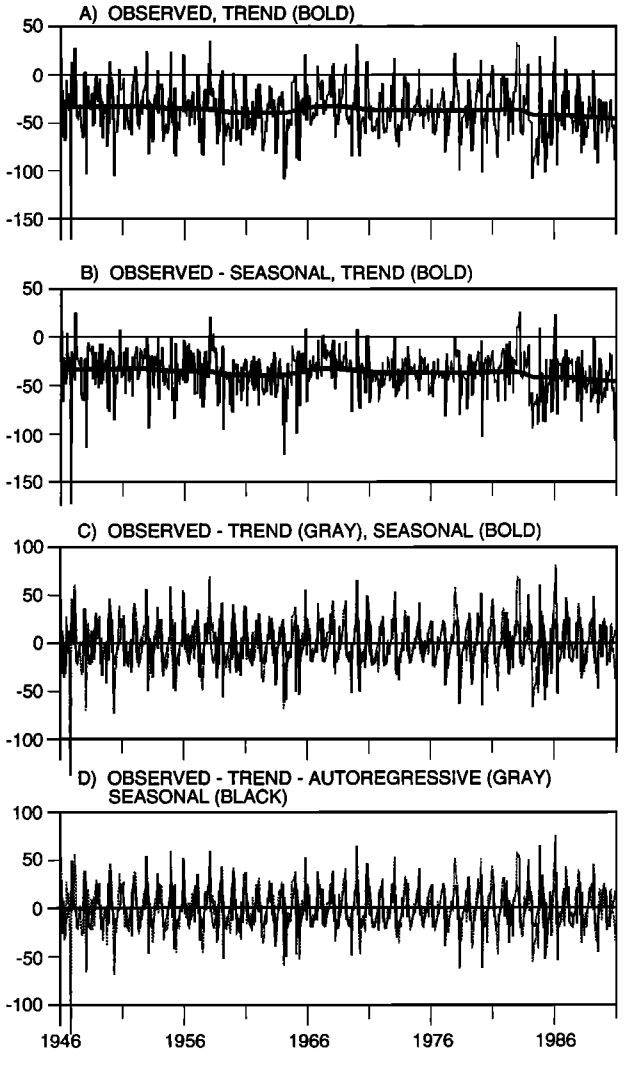

Figure 2. Comparison of COADS 37N (36–38°N) SST (°C) monthly observations to model results, for period 1946–1990. a) Overlay of trend model component (bold line) and observed monthly series. b) Overlay of trend model component (bold line) and observed series minus seasonal model component. c) Overlay of seasonal model component (bold line) and observed series minus trend model component. d) Overlay of seasonal model component and observed series minus trend and AR(1) model components.

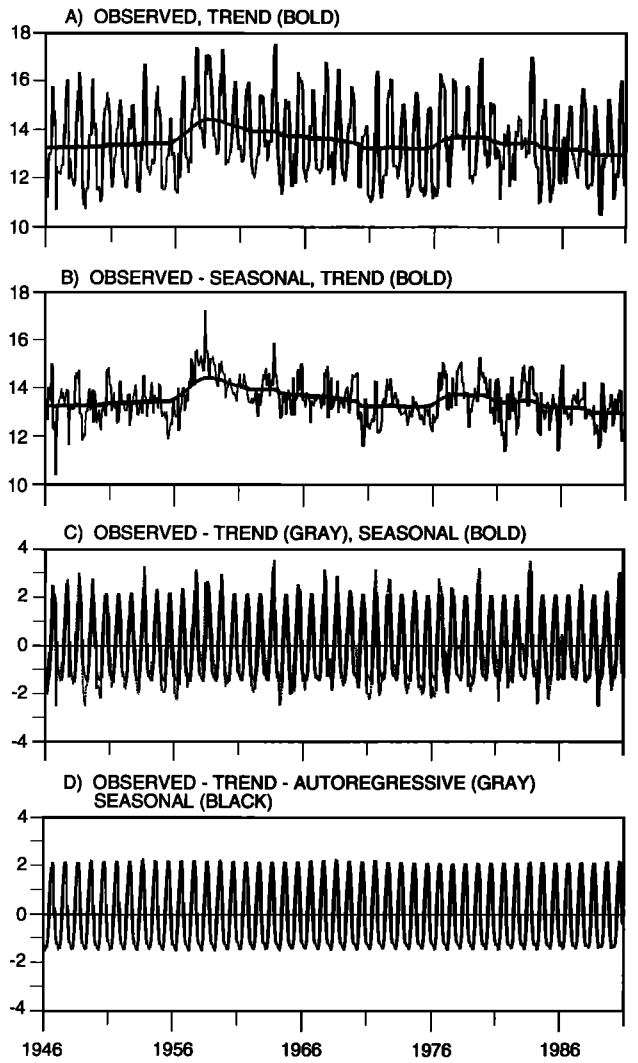

Figure 3. Comparison of COADS 37N (36–38°N) poleward wind stress (m^2/s^2) monthly observations to model results, for period 1946–1990. a) Overlay of trend model component (bold line) and observed monthly series. b) Overlay of trend model component (bold line) and observed series minus seasonal model component. c) Overlay of seasonal model component (bold line) and observed series minus trend model component. d) Overlay of seasonal model component and observed series minus trend and AR(1) model components.

trend and AR(1) components are removed, the partial residual series (Figure 2d, gray line) and the estimated seasonal component are very close, except for an extremely small error term (difference between black and gray lines in Figure 2d). This is consistent with what is known about SST, a clearly defined trend, a strong seasonal component, and highly autocorrelated with relatively little independent month-to-month variation.

The partial residual series reveals the principal differences between SST and northward wind stress series. The monthly-averaged wind stress observations are "noisy" (Figure 3a), so that removing the seasonal component makes the trend term only slightly clearer (Figure 3b). Removing the trend from the observations again produces a zero-mean series (Figure 3c), but even with the AR(1) and the trend term removed (Figure 3d), the partial residual is quite variable relative to the estimated seasonal component. Again, this seems consistent with what is known about wind stress, namely, there is a high degree of uncorrelated (month–annual) variability in the winds, but superimposed on this is a fairly regular seasonal component.

The means of the seasonal model time series for April–July (the upwelling "season") were calculated in each calendar year to produce the time series analyzed and described below (i.e., each annual value represents the average of the April–July period in that year). These series will henceforth be referred to as the upwelling time series.

3. Results

3.1. Seasonal Cycles

Average annual cycles were determined from COADS wind stress and SST seasonal model results (Figure 4). As these are detrended signals, the absolute value for any month does not necessarily represent the observed wind direction, which is equatorward throughout the year in the region south of 40°N [*Bakun and Nelson,* 1991]. Otherwise, the geographical patterns of the annual cycles agree quite well in amplitude and phase with those described earlier by *Bakun and Nelson* [1977] and *Hickey* [1979] using COADS data, as well as from calculated and measured winds and SSTs during SuperCODE [*Strub et al.,* 1987] and more recently from analysis of 10 years of buoy winds and SSTs [*Dorman and Winant,* 1995]. The close agreement between the seasonal means presented here and in these previous analyses supports our view that the model effectively separates time series into seasonal and nonseasonal components.

The annual cycle of wind stress displays two distinct regimes. The area south of 32°N features a relatively small annual amplitude with minimum (greatest equatorward) stress in early spring and a rapid transition to the weakest equatorward stress in July. Stress in the Southern California Bight has no annual signal. The seasonal cycle north of 32°N increases dramatically in amplitude. The maximum occurs in winter and the minimum occurs in June and July. In contrast to the southern region, the period of greatest equatorward stress north of the Bight occurs in the April–July "upwelling" season (the shaded area in Figure 4).

The annual amplitude in the model seasonal SST series is smallest off northern and central California (34–42°N), where coastal upwelling in spring and summer reduces the impact of seasonal warming. This also results in an April temperature minimum and September maximum off central California. Stations off southern California and the northwestern United States have higher annual amplitudes, with a February minimum and August maximum. Highest annual SST south of the Bight is in August; the minimum shifts to the south

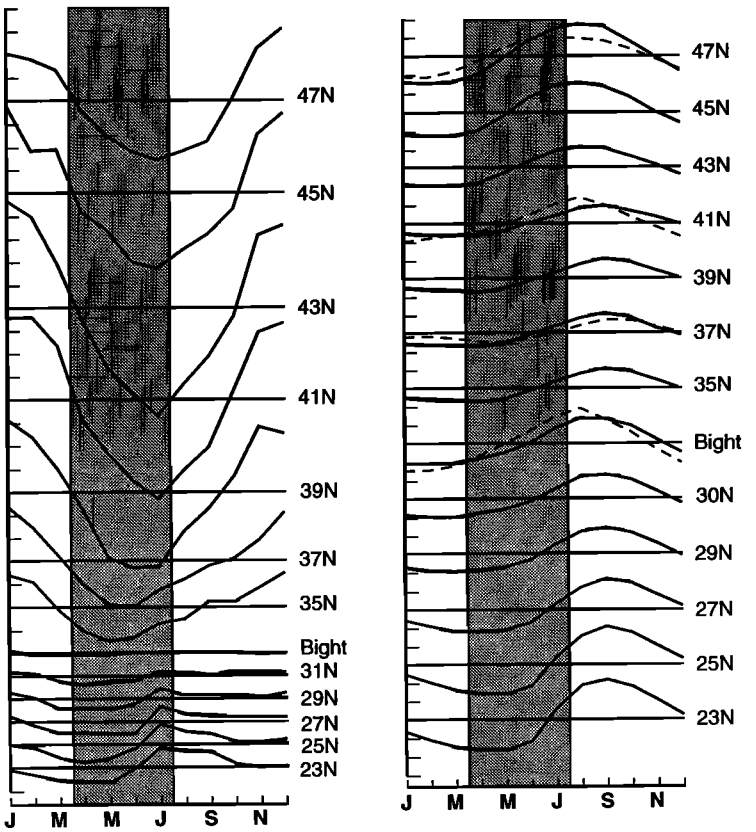

Figure 4. (left) Annual poleward wind stress and (right) SST cycles, for COADS 2° boxes, based on averages of seasonal model components. Hatched area denotes April–July period defined as upwelling season. Dashed lines denote annual cycles for selected coastal SST series. Large tick marks on vertical axes denote 10 m^2/s^2 and 2°C for stress and SST, respectively.

from March to May. The "delayed" SST maxima off Baja and central California are due to coastal upwelling, which counters seasonal warming. The coastal SST cycles (dashed lines in Figures 4 and 5) agree very well with the annual cycles of the adjacent offshore COADS boxes.

The seasonal SSS amplitude is greatest off northern California (Figure 5). Compare this to the very small amplitude at La Jolla and the reduced amplitude at Farallon. Farallon SSS is minimum in January–February and maximum in June–July. As with SST, this is related to the importance of seasonal upwelling in this region. Other stations have January minima and August maxima in SSS, in phase with SST.

The seasonal SL signal in the CCS is controlled by a combination of steric (ocean warming) and wind-forced (upwelling/downwelling) effects. SL along southern and central California is minimum in spring and maximum in September, in phase with SST. The signal at higher latitudes lags SL to the south by a few months. SL is nearly out of phase with SST and SSS at Neah Bay. The annual amplitude increases with latitude as well. The seasonal cycles of all three ocean variables described here are relatively small in amplitude along the central California coast, reflecting the mitigating effect of coastal upwelling in spring and summer on other sources of annual variability (e.g., seasonal warming, freshwater discharge). This is consistent with the occurrence of the highest seasonal amplitudes in poleward wind stress at these latitudes. The mean annual cycles of SL agree with those of *Strub et al.* [1987].

3.2. Upwelling Time Series

The mean wind stress and SST for April–July (the upwelling "season") were calculated for each year from the seasonal model series for the COADS 2° boxes, and plotted as upwelling time series (Figure 6). In most boxes there is a close positive correlation between stress and SST (Table 2). There also is considerable consistency in stress and SST between adjacent boxes.

Seasonal series over most of the CCS region south of about 40°N display a fairly linear tendency of increasing equatorward (more negative) stress and decreasing SST over time. Both tendencies reverse north of 40°N, although stress again becomes more equatorward over time north of 44°N. The relationship between stress and SST is generally negative north of 40°N (Figure 6, Table 2). South of 30°N the pattern of decreasing stress and SST changes gradually from a "bowl-shaped" series to a linear increasing trend, similar to that noted north of 40°N.

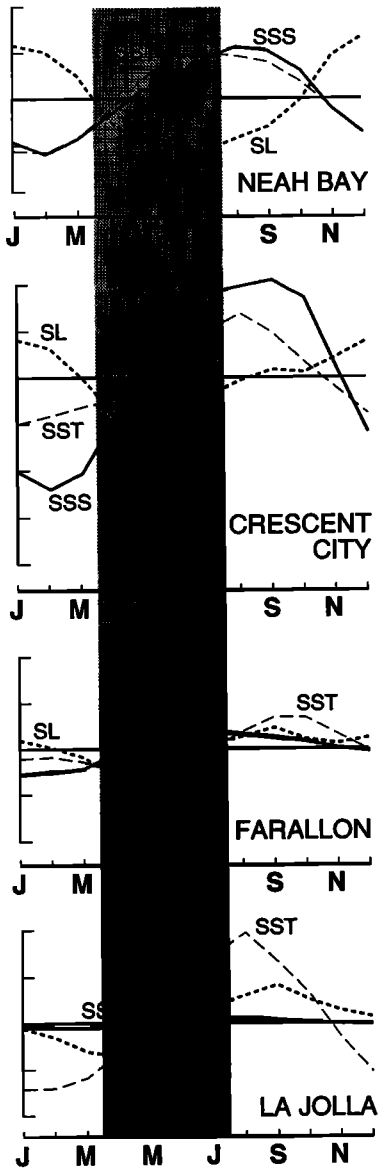

Figure 5. Annual cycles of coastal SST (dashed line), salinity (SSS, solid line), and sea level (SL, dotted line), for Neah Bay, Crescent City, Farallon, and La Jolla, based on averages of seasonal model components. Hatched area denotes April–July period defined as upwelling season. Large tick marks on vertical axes denote 2°C, 1 ppt, and .01 m for SST, salinity, and sea level, respectively.

Rajagopalan and Lall [1995] and *Thomson* [1995] use different methods to demonstrate long-term shifts in the phase of seasonal patterns in precipitation and temperature, respectively. Unlike their results, however, the majority of CCS seasonal series displayed a phase constancy; e.g., the annual maximum or minimum occurred in the same calendar month over time. With only a few exceptions, phase shifts were no more than 1 month and occurred within the April-July period. Thus the tendencies shown here are due to changes in the magnitude rather than phase of the seasonal cycle.

In summary, upwelling wind stress has become more strongly equatorward over time in the region 32–40°N and north of 44°N. SST has become cooler during the upwelling season between 30 and 40°N. The linear relationship between stress and SST is positive south of 40°N. Over the region 32–40°N, from about the U.S.–Mexico border to Cape Mendocino (the shaded region in Figure 7), the strong linear relationships between stress, SST and time are all consistent with increased upwelling.

3.3. Comparison of Shore-Based Seasonal Series to the COADS Series

All coastal SST and SL upwelling series decreased over time and all SSS series increased over time, implying an increase in upwelling (Figure 8, Table 3). The

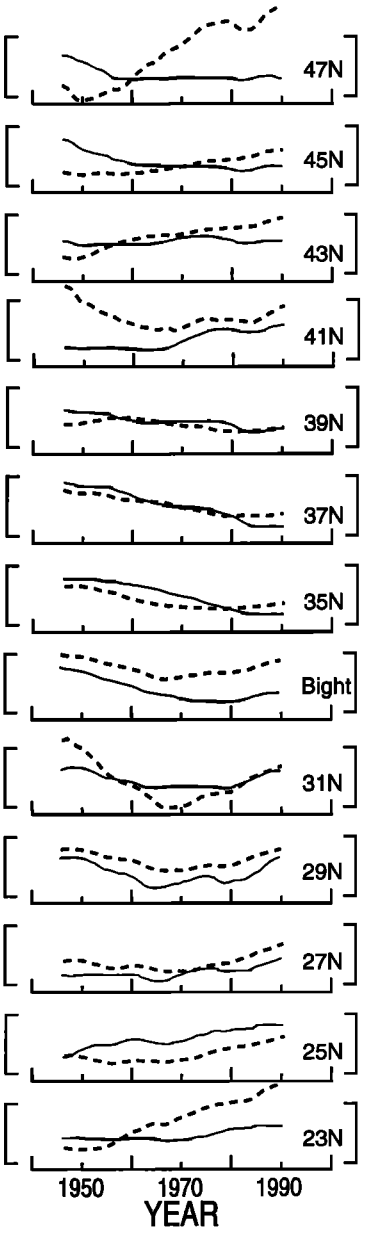

Figure 6. Time series plots of upwelling series (April–July averages from California Current System seasonal model components) for poleward wind stress (solid lines) and SST (dashed lines), for COADS 2° boxes. Vertical axes denote 3 m^2/s^2 and 0.1°C, respectively.

Table 2. Correlations (r) and Slopes (b) of Linear Fits ($y = a + bx$) of Averaged April-July Upwelling Series for Northward Wind Stress (τ) (m^2/s^2) Against Year, SST (°C) Against Year, and SST Against Northward Stress, and SST Against Northward Stress for October-January Series, for Period 1946-1990 for 2°COADS Data

Latitude	τ Versus Year (April-July)		SST Versus Year (April-July)		SST Versus τ (April-July)		SST Versus τ (October-January)	
	r	b (10^{-2})	r	b (10^{-3})	r	b (10^{-2})	r	b (10^{-2})
46-48	-0.670†	-1.805± 0.785	0.966	3.865± 0.405	-0.602	-8.937± 4.659	0.315	1.016± 1.215
44-46	-0.834†	-2.625± 0.681	0.958	0.968± 0.144	-0.646	-2.073± 0.963	0.922†	1.172± 0.196
42-44	0.469	0.500± 0.370	0.969	1.427± 0.142	0.484†	6.682± 4.748	-0.570	-1.781± 1.020
40-42	0.897	3.061± 0.592	-0.380	-0.256± 0.247	-0.037	-0.073± 0.783	0.371	6.596± 6.564
38-40*	-0.923†	-2.271± 0.372	-0.791†	-0.489± 0.149	0.631†	1.587± 0.266	0.472†	2.252± 0.167
36-38*	-0.992†	-5.556± 0.284	-0.975†	-1.126± 0.100	0.958†	1.976± 0.231	-0.720	-2.661± 1.019
34-36*	-0.986†	-5.130± 0.343	-0.852†	-0.894± 0.216	0.814†	1.642± 0.461	-0.294	-5.270± 6.800
Bight*	-0.850†	-3.686± 0.897	-0.436†	-0.414± 0.335	0.819†	1.790± 0.493	0.092	0.671± 2.902
30-32	-0.378	-1.053± 1.014	-0.433†	-1.100± 0.900	0.945†	8.605± 1.175	-0.147	-1.040± 2.786
28-30	-0.338	-1.296± 1.416	-0.275	-0.264± 0.140	0.950†	2.374± 0.306	0.334	0.446± 0.501
26-28	0.710	1.399± 0.545	0.507	0.461± 0.308	0.789†	3.644± 1.113	0.257	0.935± 1.399
24-26	0.953	3.263± 0.406	0.801	0.794± 0.233	0.780†	2.261± 0.712	0.602†	1.200± 0.633
22-24	0.809	1.627± 0.465	0.992	2.658± 0.130	0.803†	10.700± 3.116	0.816†	4.129± 1.161

Dependent (y) variable listed first. The 99% confidence intervals are given. The 0.01 (0.05) significance level on r is 0.397 (0.302), n=45 for April-July series; 0.402 (0.306), n=44 for October-January series.

† Linear regression is significant at 0.01 level, and of the sign consistent with increased upwelling (decreasing τ, SST over time; decreasing SST versus τ).

* Regions where all three linear regressions are significant and of the sign consistent with increased upwelling.

magnitude of their changes corresponds to about 0.07–0.14°C, 0.01–0.1 ppt, and 0.1–0.7 cm, respectively, over the past 45 years. Except for Crescent City, where the adjacent COADS stress (41N) shows an increasing seasonal trend, SST and SL (SSS) are positively (negatively) correlated with local wind stress (Table 4).

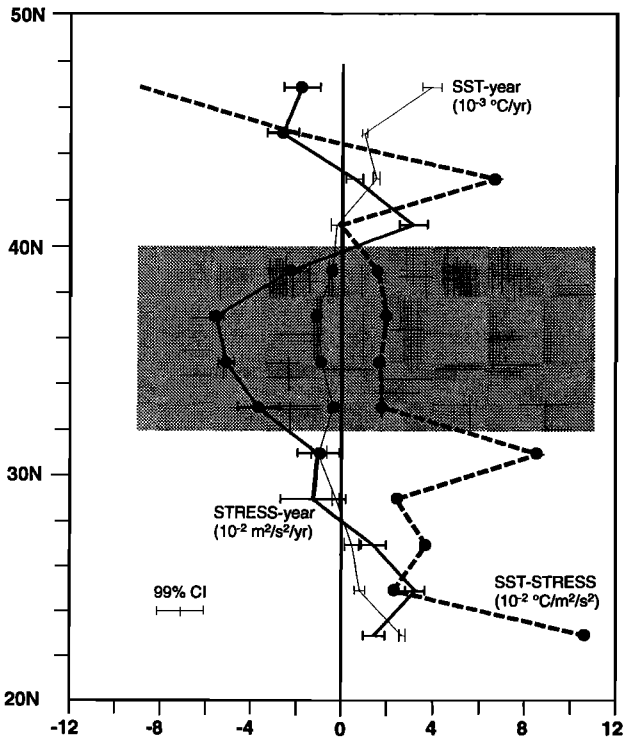

Tendencies occurring during the period covered by the COADS data (1946–1990) are consistent with those for the full-length shore series (57–78 years) (Table 5). Regressions between coastal SST, SSS, and SL (the series shown in Figure 8) are of the sign consistent with that expected if upwelling is the controlling process (Table 6).

Examination of the April–July seasonal averages at other coastal stations reveals a very similar pattern (Figure 9). Note the high degree of visual correlation between coastal SST series along the entire coast. Several stations along the central and southern California coast, over the 32–40°N range of increased upwelling suggested by the COADS data, feature decreasing SST and increasing SSS. These time series agree quantitatively with the coastal sites discussed previously, both in the linear tendency and the decadal period fluctuations. Upwelling SST and SSS series generated for coastal

Figure 7. Slopes (b) of linear fits ($y = a + bx$) of averaged April–July upwelling series values for northward wind stress (m^2/s^2) against year (bold solid line), SST (°C) against year (light solid line), and SST against northward wind stress (dashed line), for period 1946–1990 for 2° COADS data. The 99% confidence intervals (CI) are shown. Solid circles denote linear regression is significant at 0.05 level. Shading denotes region where all three linear regressions for a COADS box are significant and of the sign consistent with increased upwelling. Horizontal axis is 10^{-3} $m^2/s^2/yr$ for stress versus time, 10^{-3}°C/yr for SST versus time, and 10^{-2}°C/m^2/s^2 for SST versus stress.

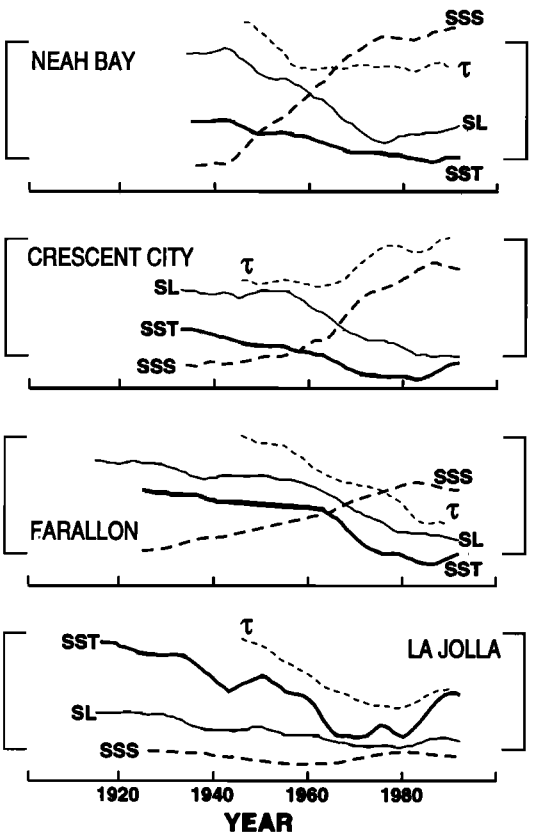

Figure 8. Time series plots of upwelling series (April–July averages from seasonal model components) for shore SST (bold solid lines), sea level (SL, light solid lines), surface salinity (SSS, bold dashed lines), and COADS poleward wind stress (τ, light dotted lines), for Neah Bay, Washington (versus 47N τ), Crescent City, California (versus 41N τ), Farallon, California (versus 37N τ), and La Jolla, California (versus Bight τ). Vertical axes denote 0.2°C, 0.1 ppt, 0.01 m, and 3 m^2/s^2, respectively. Refer to Figure 1 for location of shore stations.

stations north of 50°N (e.g., Cape St. James, British Columbia; Seward, Alaska) display no change over time, suggesting the patterns of increased upwelling noted in the CCS are not evident in the subarctic Pacific region influenced by the Alaskan Gyre.

The slopes of the linear regressions between shore-based SST and COADS stress series (Table 4) are larger than with the COADS SST and stress (Table 2); i.e., shore SST changes are greater than COADS SST changes. One exception is the negative correlation between the COADS and coastal SST at Neah Bay. The differences between the linear change of SST at the coast and COADS SST, which integrates SST over a large offshore area, probably are due to the dilution of coastal upwelling in the offshore domain of the COADS boxes.

To test whether the tendencies of the seasonal series are a coastal phenomenon, or possibly basinwide, upwelling series were constructed from the seasonal model components of SST and SSS time series at Ocean Station P (OSP), and SST at Ocean Station N (OSN) (Figure 1, Table 1). The increases in the OSP SST and SSS upwelling series (Figure 9, Table 5), located in the West Wind Drift, an eastward current that bifurcates into the California Current and the Alaskan Current, imply a seasonal increase in the contribution of subtropical water. This pattern does not reconcile with that seen in the CCS; thus it is not likely linked with the COADS results.

SST at OSN, located in the subtropical North Pacific well to the west of the CCS, displays a clear cooling tendency of the same magnitude as the coastal sites, and looks quite similar to coastal SST series over its relatively short (21 years) record length (Figure 9). Its position rules out changes in coastal upwelling as an explanation for this pattern. However changes in the wind curl over the eastern Pacific, which could lead to an intensification in Ekman pumping at locations remote from the coast, are a possibility. The hypothesized intensification of the thermal continental low in summer, which would contribute to increased coastal upwelling, could lead to changes in the wind gradients in the region of OSN as well. While an investigation of this possibility is beyond the scope of this paper, it is nevertheless an intriguing question, given the similarity between the coastal and OSN SST upwelling series. Closer analysis may suggest mechanisms by which long-term basin-scale forcing variability may impact up-

Table 3. Correlations (r) and Slopes (b) of Linear Fits of Averaged April-July Upwelling Series for SST (°C), SSS (ppt), and Sea Level (m) Against Year, for Selected Coastal Stations, for Period 1946-1990

Station	SST Versus Year		SSS Versus Year		SL Versus Year	
	r	b (10^{-3})	r	b (10^{-4})	r	b (10^{-4})
Neah Bay*	-0.972†	-1.362± 0.129	0.959†	24.416± 2.820	-0.919†	-1.591± 0.269
Crescent City*	-0.898†	-1.500± 0.289	0.981†	23.235± 1.794	-0.974†	-1.568± 0.143
Farallon*	-0.958†	-3.009± 0.355	0.976†	10.870± 0.955	-0.981†	-1.493± 0.116
La Jolla*	-0.566†	-1.589± 0.910	0.775†	2.219± 0.712	-0.728†	-0.300± 0.111

Dependent (y) variable listed first. The 99% confidence intervals are given. The 0.05 (0.01) significance level on r is 0.302 (0.397), n=45.

† Linear regression is significant at 0.05 level, and of the sign consistent with increased upwelling (decreasing SST and SL, increasing SSS over time).

* All three linear regressions are significant and of the sign consistent with increased upwelling at all four locations.

Table 4. Correlations (r) and Slopes (b) of Linear Fits of Averaged April-July Upwelling Series for Coastal SST (°C), Salinity (SSS) (ppt), and Sea Level (SL) (m) Against Northward Wind Stress (τ) (m^2/s^2) in Adjacent 2°COADS Regions, for Period 1946-1990

Station	SST Versus τ		SSS Versus τ		SL Versus τ	
	r	b (10^{-2})	r	b (10^{-3})	r	b (10^{-3})
Neah Bay*	0.656†	3.415± 1.542	-0.764†	-72.178± 23.951	0.715†	4.601± 1.766
Crescent City	-0.827	-4.047±1.082	0.936	64.961± 9.596	-0.890†	-4.200± 0.844
Farallon*	0.944†	11.282± 0.729	-0.966†	-1.920± 0.202	0.971†	2.638± 0.256
La Jolla*	0.892†	5.777± 1.150	-0.645†	-4.264± 1.983	0.966†	0.918± 0.097

Dependent (y) variable listed first. Results shown for Neah Bay, Washington (versus 47N τ), Crescent City, California (versus 41N τ), Farallon, California (versus 37N τ), and La Jolla, California (versus Bight τ). The 99% confidence intervals are given. The 0.05 (0.01) significance level on r is 0.302 (0.397), n=45.

† Linear regression is significant at 0.05 level, and of the sign consistent with increased upwelling (increasing SST and SL, decreasing SSS, versus τ).

* Locations where all three linear regressions are significant and of the sign consistent with increased upwelling.

per ocean circulation patterns, and possibly coastal upwelling processes.

While the majority of the upwelling series display a highly linear tendency over time, some series exhibit considerable variability on decadal scales that is consistent within adjacent areas. For example, shore SSTs shift suddenly to more rapid cooling in the early 1960s, to a slower rate of decreasing SST a few years later, and appear to reverse around 1980 (Figure 9); SSS shows the opposite pattern. Nonlinear upwelling series should not be construed as lacking a climate signal. Climate variability is not monotonic (e.g., the dramatic 1976 climate shift over the north Pacific [*Trenberth,* 1990; *Graham,* 1994; *Trenberth and Hurrell,* 1994]). Many of the series have variability such that truncating their length by even a few years leads to substantially different linear tendencies. A key result here is their consistency within geographical regions, such as the 32–40°N area dominated by coastal upwelling.

4. Discussion

Strong evidence of a systematic intensification of upwelling during April–July is seen along the west coast of North America between 32° and 40°N (Figure 7, Table 2). This region corresponds with an area where coastal upwelling predominates during spring and summer [cf. *Parrish et al.,* 1981]. It is offset slightly south of the primary upwelling region (Point Conception, California to Cape Blanco, Oregon), suggesting that southward advection may account for the distribution of some of the cooling tendencies in COADS SSTs. This is consistent with the small negative SST-stress slope at 41N, at the northern edge of the upwelling region, as well as the relatively large positive slope at 31N, the southern boundary of upwelling (Figure 7). Another large positive slope is seen at 23N, south of an upwelling center off Baja California [*Bakun and Nelson,* 1977].

SST during the upwelling season has increased north and south of this region of intensified upwelling. However, a corresponding decrease in equatorward stress, implying decreased coastal upwelling, only occurs south of 28°N. Stress is negatively correlated with SST north of 40°N, suggesting that seasonal changes in wind stress are not reflected in SST through coastal upwelling. This is not surprising since this region is at the northern extent of predominantly meridional wind associated with the pressure gradient between the continental low over

Table 5. As for Table 3, for Entire Data Set Available

Station	SST Versus Year		SSS Versus Year		SL Versus Year	
	r	b (10^{-3})	r	b (10^{-4})	r	b (10^{-4})
Neah Bay*	-0.976†	-1.378± 0.105 (58)	0.993†	38.379± 1.798 (44)	-0.943†	-1.569± 0.189 (59)
Crescent City*	-0.926†	-1.473± 0.204 (60)	0.928†	11.942± 1.867 (46)	-0.949†	-1.205± 0.135 (60)
Farallon*	-0.942†	-2.124± 0.240 (68)	0.985†	9.760± 0.540 (68)	-0.949†	-0.953± 0.093 (78)
La Jolla	-0.853†	-2.028± 0.369 (77)	-0.068	-0.131± 0.615 (67)	-0.920†	-0.403± 0.051 (78)
OSP	0.581	0.859± 0.484 (43)	0.844†	1.173± 0.325 (37)		
OSN	-0.881†	-3.285± 1.043 (21)				

Length of each series in years shown in parentheses next to 95% confidence interval.

† Linear regression is significant at 0.05 level, and of the sign consistent with increased upwelling (decreasing SST and SL, increasing SSS over time).

* All three linear regressions are significant and of the sign consistent with increased upwelling at all four locations.

Table 6. Correlations (r) and Slopes (b) of Linear Fits of Averaged April-July Upwelling Series for COADS SST (CSST) (°C), Coastal SST (°C), SSS (ppt), and Sea Level (m), for Period 1946-1990

Station	CSST Versus SST		SSS Versus SST		SST Versus SL		SSS Versus SL	
	r	b	r	b	r	b	r	b
Neah Bay	-0.963	-2.745± 0.304	-0.977*	-1.774± 0.153	0.962*	7.778± 0.871	-0.985*	-14.464± 1.007
Crescent City	0.497*	0.203± 0.139	-0.933*	-1.323± 0.200	0.945*	9.809± 1.330	-0.988*	-14.540± 0.881
Farallon	0.972*	0.357± 0.034	-0.978*	-0.347± 0.029	0.989*	20.410± 1.219	-0.988*	-7.226± 0.453
La Jolla	0.950*	0.320± 0.041	-0.442*	-0.045± 0.036	0.943*	64.292± 8.862	-0.602*	-4.190± 2.179

Dependent (y) variable listed first. Results shown for Neah Bay, Washington (versus 47N CSST), Crescent City, California (versus 41N CSST), Farallon, California (versus 37N CSST), and La Jolla, California (versus Bight CSST). The 99% confidence intervals are given. The 0.05 (0.01) significance level on r is 0.302 (0.397), $n = 45$.

* Linear regression is significant at 0.05 level, and of the sign consistent with increased upwelling (decreasing CSST, SST and SL; increasing SSS).

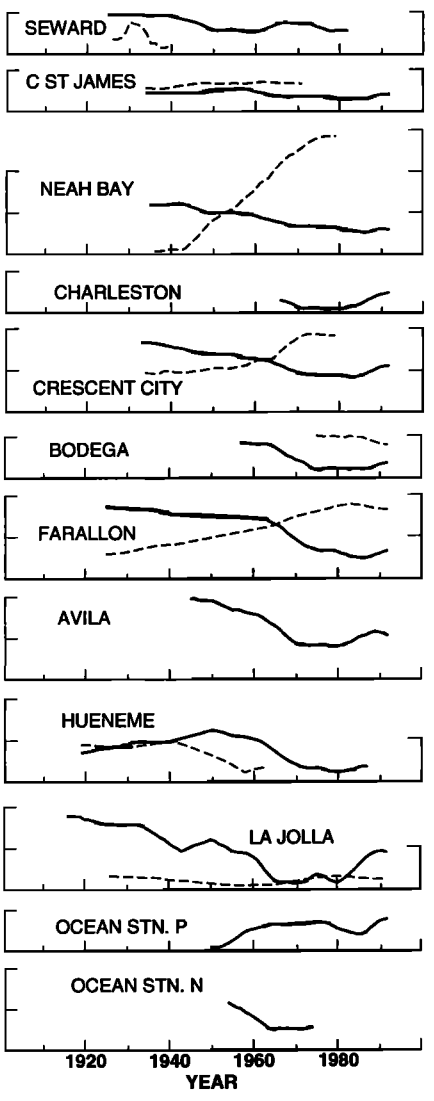

Figure 9. Time series plots of upwelling series (April–July averages from seasonal model components) for shore SST (solid lines) and SSS (dashed lines), for representative shore stations along the North American coast, and Ocean Stations N and P. Large tick marks on vertical axes denote 0.1°C and 0.05 ppt, respectively. Refer to Figure 1 for location of shore stations.

the western United States and the North Pacific High, and is more influenced by predominantly zonal wind stress in the gradient between the High and the Aleutian Low [*Bakun and Nelson,* 1991]. Offshore-directed Ekman surface transport during spring and summer is greatly reduced north of 40°N as well [*Parrish et al.,* 1983], further demonstrating the reduced role of coastal upwelling at northern latitudes.

Regions north of 40°N and south of 32°N are away from the influence of the continental low as well. *Bakun* [1992] points out that the Gulf of California occupies the area corresponding to the continental interior at higher latitudes. Therefore these areas are less susceptible to any increase in upwelling that would be associated with the intensification of the summer continental low and the subsequent strengthening of equatorward wind stress. Finally, anticyclonic curl dominates in the northern and southern regions, in contrast to strong cyclonic curl off California [*Bakun and Nelson,* 1991]. Anticyclonic curl leads to Ekman convergence and downwelling, countering the effect of offshore Ekman transport and possibly explaining the limited geographical extent of the increased coastal upwelling over the past several decades. We are currently examining the relative role of wind stress and wind stress curl in driving decadal-scale changes in upwelling.

The coastal station series corroborate these results. Four shore stations; namely, Neah Bay, Crescent City, Farallon, and La Jolla, have long series of SST, SSS and SL for comparison to the COADS wind (Figure 8). Farallon is located in the center of the upwelling region on an island about 45 km west of San Francisco (SL for this location was measured at San Francisco). This site is frequently bathed by recently upwelled water from the north [cf. *Schwing et al.,* 1991]. An increasing equatorward wind stress corresponds with decreasing SST and SL, and increasing SSS at this location, all consistent with a systematic intensification of upwelling over the past several decades.

The tendencies at Neah Bay are similar to those at Farallon. The same is true at La Jolla; however, the rate of change in the series over time is reduced. Coastal upwelling may be increasing in the Bight, but it is either

a relatively small change or may be partially masked by other factors that impact the seasonality of the dynamics controlling the Bight's oceanic conditions. At Crescent City the oceanic variables change in a manner consistent with increased upwelling, despite the fact that wind stress at this latitude has become increasingly poleward. The COADS winds may not be truly representative of the nearshore winds that drive coastal upwelling. Another possibility is that ocean conditions off northern California are controlled by nonlocal forcing which advects upwelled water south from the Cape Blanco upwelling region. Crescent City is near the divergence point of both the mean wind stress and the tendency of the COADS upwelling series. Ongoing analysis of wind and SST trends suggests further that the area's wind and SST fields are extremely heterogeneous on space scales of $O(100$ km) at timescales of years to decades (R. H. Parrish, personal communication, 1996), which suggest a combination of nonlocal forcing and complex circulation may be responsible for the seasonal tendencies seen at Crescent City.

Are the seasonal tendencies in wind stress and SST truly limited to the upwelling season, or are they representative of a pattern that occurs throughout the year? The former should be the case, since nonseasonal tendencies will be incorporated into the trend model component. Time series were constructed from the October–January means of the seasonal model series. The slopes of the linear fits of COADS SST to wind stress for these winter seasonal series (Table 2) show a very different pattern from the upwelling season. Only a few isolated COADS boxes reflect a positive relationship between SST and stress. Of these, a positive correlation was found for only one box within the 32–40°N upwelling area (39N), and this was associated with increasing (reduced upwelling) SST and stress tendencies. From this it can be concluded that the patterns consistent with increasing upwelling are limited to the spring and summer. Other physical processes are controlling the seasonal wind and SST tendencies at other times of the year.

Are the regression statistics described above unique to the seasonal model components? The analysis was repeated by examining time series constructed from the April–July averages of the model trends and the monthly observations (raw data); e.g., Figures 2a and 3a, bold and light lines, respectively. The series constructed from the observations are analogous to those analyzed by *Bakun* [1990]. The wind stress trend series display an increasing equatorward tendency south of 42°N and poleward north of 42°N, a pattern matched by the April–July observations (Figure 10). The tendencies of the observed and trend series are negative, consistent with the seasonal upwelling series in the region 32–40°N (but with larger confidence intervals). However, the linear slopes of the trends and observations (0.1–0.6 $m^2/s^2/yr$) are generally an order of magnitude greater than in the seasonal tendencies (0.01–0.05 $m^2/s^2/yr$), reflecting the strong bias of the April–July observations toward the long-term trend. Linear tendencies of the CCS geostrophic wind series constructed by *Bakun* [1990] for April–September are very similar

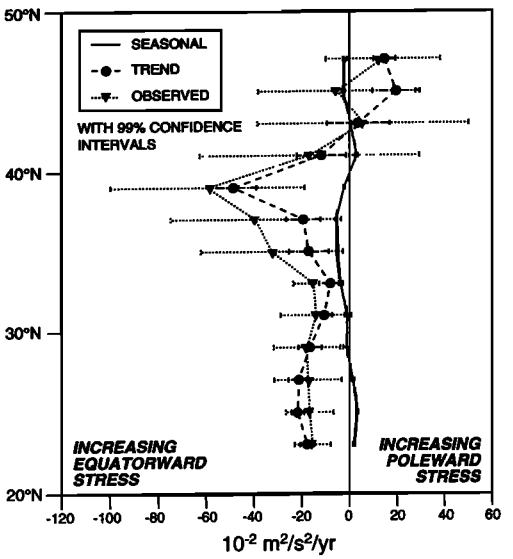

Figure 10. Slopes (b) of linear fits ($y = a+bx$) of averaged California Current April–July values of 2° COADS data poleward wind stress (m^2/s^2) against year, from monthly observations (dotted line), trend model component (dashed line), and seasonal model component (solid line), for period 1946–1990. The 99% confidence intervals are shown.

to the trend and observation tendencies reported here, reflecting the fact that long-term trends were incorporated in the "seasonal" series used in his analysis.

The April–July trend and observed series south of 36°N display a general warming pattern (Figure 11), whereas the seasonal upwelling series show a cooling tendency over the region 28–42°N. The wind and SST trend series have a strong positive correlation only at 39N, which is also the only location where the SST trends have a significant cooling tendency. As with stress, the linear tendencies of the SST trends are $O(10)$ and greater than the seasonal tendencies, and generally of opposite sign. Again the observation and trend series correspond closely. The seasonal SST component off much of California and Baja has been cooling at a rate of $-0.5--1.0 \times 10^{-3}$°C/yr, while the trends in this area exhibit a warming tendency of greater than 10×10^{-3}°C/yr. *Schwing* [1994] found consistent results from a similar comparison of the Farallon SST and SSS observed, trend, and seasonal series. The long-term warming trend masks seasonal cooling associated with increased upwelling during spring and summer off central and southern California. These comparisons reflect the importance of using a method that separates seasonal and long-term contributions to environmental time series, and argue against looking for changing seasonal patterns in direct extractions from observations without properly accounting for the nonlinear climate trend. Otherwise long-term climate patterns may be improperly linked to, and even misidentified as, changes in the seasonal cycle.

Roemmich and McGowan [1995] have found that SSTs off southern California have warmed by more than 1.5°C since 1951, despite a slight increase in equatorward wind

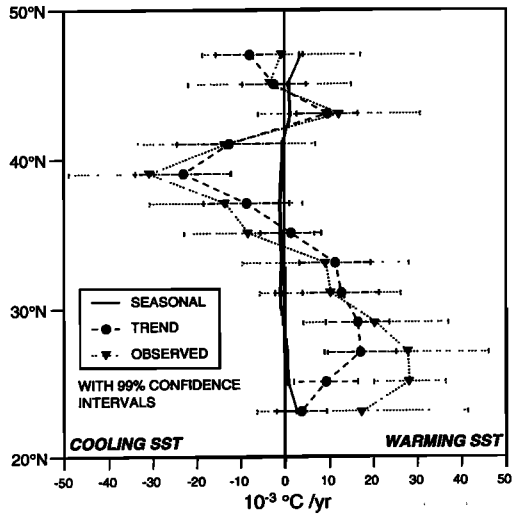

Figure 11. Slopes (b) of linear fits ($y = a + bx$) of averaged California Current April–July values of 2° COADS SST (°C) against year, from monthly observations (dotted line), trend model component (dashed line), and seasonal model component (solid line), for period 1946–1990. The 99% confidence intervals are shown.

stress over that time. While this relationship appears to contradict our results, it is because the model we apply separates the seasonal component described here from the series' trends, which are fundamentally what Roemmich and McGowan as well as *Bakun* [1990] report. In fact, the 43-year trend reported by Roemmich and McGowan (3.5×10^{-2}°C/yr) is similar to our model trends for southern California (Figure 11), lending further credence to our ability to separate the seasonal and nonseasonal elements of environmental series. It is essential to recognize the difference between changes in the model trends, which are due to superannual changes over time, and changes in the seasonal series, which are associated with climate variations that favorably affect a certain season or portion of the year.

Similarly, the long-term rates of change in seasonal SST (Table 2) and SL (Tables 3 and 5) for the Southern California Bight are only about one-tenth the magnitude of the tendencies calculated by *Roemmich* [1992], and are of opposite sign (i.e., Roemmich's trends imply warmer SST and higher SL). Paradoxically, the estimated linear seasonal change of 0.1–0.64°C per cm of SL change (Table 6) is similar to the ratio of La Jolla SST to SL (0.2–0.7°C/cm) derived from trends provided by Roemmich. Therefore the baroclinic dynamic effect of seasonal upwelling on sea level is similar in magnitude to the steric effect of long-term warming of the upper ocean.

Wind-driven coastal upwelling is one of several processes that control SST and other ocean conditions; other factors that may affect upper ocean variability (e.g., global warming) cannot be ignored. The importance of these effects relative to local wind forcing differs as a function of timescale, which may account for the different relationship between stress and SST in the trend and seasonal model components. Specifically, we conclude that variations in coastal upwelling controls SST over much of the CCS on seasonal scales. Therefore a close relationship exists between the spring/summer seasonal stress and SST series. SST trends, on the other hand, appear unrelated to changes in local wind stress because factors in addition to wind forcing contribute significantly to SST long-term variability [*Cayan*, 1992].

The relationships between wind stress, SST, SSS, and SL qualitatively suggest increased upwelling along the U.S. west coast over the previous several decades. We now examine how well these temporal tendencies agree quantitatively, based on the dynamic balances that describe coastal upwelling and circulation. These are merely order of magnitude estimates of the dynamical relationships, and do not account for changes in ocean structure due to changes in temperature throughout the upper water column (e.g., mixed layer depth) or redistribution of water masses. This discussion also is based on highly simplified dynamical balances and assumptions. A more complete theoretical treatment is merited; nevertheless the relationships described below are consistent between the variables we have modeled, and with our premise of increased upwelling.

Consider the relationship between increasing equatorward wind stress and lowering coastal sea level. The regression slope between Farallon (i.e., San Francisco) SL and 37N wind pseudo-stress is 2.6×10^{-3} m/m^2/s^2 (Table 4). Converting this parameter to stress units (Pa), using a drag coefficient of 0.0026 [following *Bakun and Nelson*, 1991], gives a slope of 0.8 m/Pa. This value is within the range of the quasi-steady response of SL to alongshelf wind stress off central California, estimated from observations (> 0.2 m/Pa by *Denbo and Allen* [1987]) and theory (0.4 m/Pa by *Brink et al.* [1987]).

Next consider the rates by which surface temperature and salinity might change in concert with lowering sea level if upwelling is increasing. For a stratified ocean, the internal ocean adjusts to displacements of the sea surface in a ratio proportional to $\Delta\rho = (\rho_L - \rho_U)/\rho_L$, the difference in the density of the lower (ρ_L) and upper (ρ_U) layers, divided by the lower layer density. $\Delta\rho$ is of the order of 10^{-3} for the CCS. Multiplying the vertical gradients of temperature (SST_z) and salinity (SSS_z) by the rate of uplift for the interior gives the rate at which isotherms and isohalines are outcropping, i.e., the rate of change in surface temperature and salinity. The time rate of change of SST (SST_t) and SSS (SSS_t) is related to changes in the sea surface height (SL_t) by

$$SST_t = \frac{SL_t\, SST_z}{\Delta\rho} \qquad SSS_t = \frac{SL_t\, SSS_z}{\Delta\rho}, \quad (11)$$

From Table 3, the slopes of the linear regression of SL over time, $SL_t = O(-10^{-4}$ m/yr). Spring and summer $SST_z = -10^{-2}$ - -10^{-1}°C/m and $SSS_z = 10^{-3}$–10^{-2} ppt/m off central California [*Sakuma et al.*, 1994]. From equation (11), $SST_t = -10^{-3}$ - -10^{-2}°C/yr and $SSS_t = 10^{-4}$–10^{-3} ppt/yr, which compare favorably to the rates of change of Farallon SST and SSS (-3×10^{-3}°C/yr and 1.5×10^{-4} ppt/yr, respectively) (Table 3).

As a final quantitative check of the results, we estimate the temporal change in cross-shore Ekman surface transport and calculate how vertical velocities in the CCS may be changing over time. Cross-shelf Ekman transport is

$$uh = \tau^y/\rho f \tag{12}$$

where h is the depth of the Ekman surface layer, τ^y the along-shelf wind stress component, ρ the water density, and f the Coriolis acceleration parameter. Assuming that changes in along-shelf transport are small relative to the cross-shelf transport, the vertical velocity w is given by the divergence of surface cross-shelf transport

$$w = (uh)_x \approx \left((uh)_C - (uh)_{R_i}\right)/R_i. \tag{13}$$

for $h_x \approx 0$, the divergence between transport at the coast $(uh)_C$ and at 1 Rossby radius of the coast $(uh)_{R_i}$.

Combining equations (12) and (13) and differentiating with respect to time gives $w_t = -\tau^y_t/f\rho R_i$, assuming that transport at the coastal boundary is zero. For the tendencies of τ^y along central California (about -5×10^{-2} m^2/s^2/yr from Table 2) and taking R_i=20 km, the tendency of $(uh)_{R_i} \approx -2 \times 10^{-3}$ m^2/s/yr, and the change in vertical velocity near the coast is about $+1 \times 10^{-7}$ m/s/yr, an O(0.8 cm/d) increase in upward velocity per year. *Xie and Hsieh* [1995] estimate a July upwelling temporal gradient of 0–0.5 cm/d/yr for the CCS region from 1950–1988 COADS monthly wind stress. The agreement between Xie and Hsieh's upwelling tendencies, based on monthly means of the observations, and those estimated here from the seasonal model series, suggests that long-term changes in upwelling along the west coast of North America are probably controlled by temporal shifts in vertical velocity during the upwelling season, which we surmise are due to increased equatorward wind stress and the resulting offshore Ekman transport.

The greater equatorward stress tendencies off 34–38°N, cf. further south also should lead to relatively greater offshore surface transport off central California and a long-term increase in the seasonal set-down of the alongshore pressure gradient. A linear regression of the difference between the San Francisco and San Diego (SF-SD) seasonal SL series against time gives a slope of -1.2×10^{-4} m/yr ($r = -0.96$, 99% confidence interval = 1.3×10^{-5} m/yr). The stations are about 750 km apart, giving a change in the gradient (η_{yt}) of about -1.6×10^{-10}/yr. The time-differentiated cross-shelf geostrophic velocity is $u_t = -g\eta_{yt}/f$, where g is the acceleration due to gravity. The tendency for η_y, estimated from the SF-SD SL difference, gives an onshore increase in $u_t \approx 5 \times 10^{-4}$ m^2/s/yr within a typical Ekman surface layer of 20–30 m [*Huyer*, 1983], which would decrease the change in the offshore Ekman transport by about 25%.

5. Summary

State-space models are applied to multidecadal monthly averaged time series of poleward wind stress, sea surface temperature, coastal salinity, and coastal sea level from the California Current System (CCS). The period of analysis is 1946–1990. The models estimate a nonstationary nondeterministic seasonal component, a nonparametric nonlinear trend, and an AR(1) series for each time series, using a combination of Kalman filtering and maximum likelihood methods. Our objective is to examine the variability of coastal upwelling patterns during spring and summer in the CCS. Specifically, we test the hypothesis of *Bakun* [1990] that a long-term global warming trend has led to increased equatorward wind stress along the west coast of North America, which has resulted in increased rates of coastal upwelling.

The results show a clear separation of the seasonal signal from the trend for wind stress, SST, salinity, and sea level. The utility of estimating nonstationary seasonal patterns, using the state-space models, is demonstrated with the discovery of a systematic increase in equatorward stress and salinity, and decrease in SST and sea level during spring and summer, evidence that coastal upwelling has intensified. Evidence of increased upwelling is strongest and most prevalent in areas where seasonal coastal upwelling is a dominant process (e.g., 32–40°N). This pattern of increasing upwelling over time cannot be discerned in the monthly observations or trend model series. Neither is evidence of increased upwelling found in fall-winter.

State-space models are a powerful tool for separating interannual-to-interdecadal fluctuations in environmental time series from seasonal patterns of variability. The model results help provide a better understanding of the coastal ocean's response to long-term variations in atmospheric forcing, as well as the potential contribution of natural and anthropogenic signals, and regional differences in these effects. The results presented here demonstrate the importance of evaluating temporal and spatial variability over the entire spectrum, rather than simply at global climate scales, when examining long-term environmental fluctuations. They also demonstrate the importance of considering changes in seasonal patterns independently from changes in the long-term climate trend.

Appendix: State-Space Decomposition of a Time Series

The linear state-space model that is amenable to the Kalman filter takes the form

$$y(t) = A(t)x(t) + v(t) \tag{A1a}$$

$$x(t) = \Phi x(t-1) + w(t) \tag{A1b}$$

where the observation equation (A1a) has $y(t)$, a $q \times 1$ vector of the observed data (in this case, $q = 1$), $A(t)$ is a $q \times p$ matrix which relates the data to the unobserved components $x(t)$, which is a vector of dimension $p \times 1$, and $v(t)$ is a $q \times 1$ vector of independent, identically distributed Gaussian random variables with $Ev(t) = 0$ and noise covariance matrix

$$R = E(v(t)v(t)'). \tag{A2}$$

The evolution of the unobserved components or states $x(t)$ is governed by the initial value $x(0)$ and the state equation (A1b). The matrix Φ is a $p \times p$ transition matrix, and the $p \times 1$ vector $w(t)$ is another independent, identically distributed Gaussian random variable with $E(w(t)) = 0$ and

$$Q = E(w(t)w(t)'). \tag{A3}$$

The specification of the model is completed by assuming that $x(0)$ is also Gaussian with $E(x(0)) = \mu$ and

$$\Sigma = E(x(0) - \mu)(x(0) - \mu)'. \tag{A4}$$

See *Shumway* [1988, Section 3.4] for further details on the state-space model.

Kitagawa and Gersch [1984] show how to put the smoothness priors assumptions of equations (5) and (6) into state-space form. The model for $k = 1$ and with a first-order autoregression will be given. The model for other values follows analogously. The vector $y(t)$ is a scalar, the observed value of the time series at time t. The state vector $x(t)$ is of dimension 13 and is of the form:

$$x(t)' = (T(t), S(t), \ldots, S(t-11), I(t)) \tag{A5}$$

and the transition matrix Φ is given by

$$\begin{pmatrix} 1 & 0 & 0 & \ldots & 0 & 0 \\ 0 & -1 & -1 & \ldots & -1 & 0 \\ 0 & 1 & 0 & \ldots & 0 & 0 \\ 0 & 0 & 1 & \ldots & 0 & 0 \\ \vdots & \vdots & \vdots & \ddots & \vdots & \vdots \\ 0 & 0 & 0 & \ldots & 1 & 0 \\ 0 & 0 & 0 & \ldots & 0 & \phi \end{pmatrix} \tag{A6}$$

where ϕ is the autoregressive parameter which is to be estimated. The observation matrix (from (1)) is given by

$$A = \begin{pmatrix} 1 & 1 & 0 & 0 & 0 & 0 & 0 & 0 & 0 & 0 & 0 & 0 & 1 \end{pmatrix}. \tag{A7}$$

The specification is complete by setting the observation error covariance matrix equal to $R = \sigma_e^2$ and by setting the state noise covariance matrix equal to

$$\begin{pmatrix} \sigma_T^2 & 0 & 0 & \ldots & 0 & 0 \\ 0 & \sigma_S^2 & 0 & \ldots & 0 & 0 \\ 0 & 0 & 0 & \ldots & 0 & 0 \\ \vdots & \vdots & \vdots & \vdots & \vdots & \vdots \\ 0 & 0 & 0 & \ldots & 0 & \sigma_I^2 \end{pmatrix}. \tag{A8}$$

For given values of the vector of parameters $\Theta = (\phi, \sigma_T^2, \sigma_S^2, \sigma_I^2, \sigma_e^2)$, the minimum mean-square-error estimates of each of the state vector components can be estimated using the Kalman filter and smoother. A particularly efficient form of the algorithm was developed independently by *Ansley and Kohn* [1985, 1990], *Kohn and Ansley* [1987] and *De Jong* [1989, 1990, 1991]. Both algorithms include the case where $\Sigma \to \infty$, a diffuse or noninformative prior (see above references). Let $x(t|\tau)$ denote the expected value of the state vector given the data up to and including time τ; $P(t|\tau)$ denote the covariance matrix of the state vector conditional on the data up to and including time τ; and $r(t)$ be a vector of dimension p, and $R(t)$ a $p \times p$ matrix. Then the filter and smoothing steps proceed as follows:

A1. Filtering

Initialize

$$x(0) = \mu \tag{A9a}$$
$$P(0) = \Sigma \tag{A9b}$$

Iterate for $t = 1, T$

$$e(t) = y(t) - Ax(t|t-1) \tag{A10a}$$
$$D(t) = AP(t|t-1)A + R \tag{A10b}$$
$$K(t) = \Phi P(t|t-1)A'D(t)^{-1} \tag{A10c}$$
$$x(t+1|t) = \Phi x(t|t-1) + K(t)e(t) \tag{A10d}$$
$$L(t) = \Phi - K(t)A \tag{A10e}$$
$$P(t+1|t) = \Phi P(t|t-1)L(t)' + Q \tag{A10f}$$

A2. Smoothing

Initialize

$$r(T) = 0$$
$$R(T) = 0$$

Iterate for $t = T-1, 0$

$$r(t-1) = A'D(t)^{-1}e(t) + L(t)'r(t)$$
$$R(t-1) = A'D(t)^{-1}A + L(t)'R(t)L(t)$$
$$x(t|T) = x(t|t-1) + P(t|t-1)r(t-1)$$
$$P(t|T) = P(t|t-1) + \\ + P(t|t-1)R(t-1)P(t|t-1)$$

The log-likelihood $L(Y;\Theta)$ given all the data Y and the parameter vector Θ is given by [e.g., *Shumway*, 1988, page 178]

$$\ln L(Y;\Theta) = -\frac{1}{2}\sum_{t=1}^{T} \ln |D(t)| - \frac{1}{2}\sum_{t=1}^{T} e(t)'D(t)^{-1}e(t).$$

To use the EM algorithm [*Dempster et al.*, 1977] it is necessary to derive the complete data likelihood; here the components $x(t)$ are viewed as unobserved or "missing." After some manipulation, this can be shown to be [*Shumway*, 1988, page 179] where the terms $S_t(0)$,$S_t(1)$, and $S_{t-1}(0)$ are defined as

$$S_t(0) = \sum_{t=1}^{T}(P(t|T) + x(t|T)x(t|T)')$$
$$S_{t-1}(0) = \sum_{t=0}^{T-1}(P(t1|T) + x(t|T)x(t|T)')$$
$$S_t(1) = \sum_{t=1}^{T}(P(t,t-1|T) + \\ + x(t|T)x(t-1|T)') \tag{A11}$$

and

$$P(t,t-1|T) = E[(x(t)-x(t|T))(x(t-1) -x(t-1|T))'|y(1),\ldots,y(T)].$$

A recursion for $P(t,t-1|T)$ is given by *Shumway and Stoffer* [1982] and *De Jong* [1990]. The complete data likelihood is maximized by setting

$$\begin{aligned}\Phi &= S_t(1)[S_{t-1}(0)]^{-1}\\ Q &= T^{-1}[S_t(0) - S_t(1)\Phi' - \Phi S_t(1)' + \Phi S_{t-1}(0)\Phi']\\ R &= T^{-1}\sum_{t=1}^{T}[(y(t)-Ax(t|T))(y(t)-Ax(t|T))' +AP(t|T)A'].\end{aligned} \quad \text{(A12)}$$

In the model applied in this paper, since most of Φ is fixed, the new estimate of ϕ is the (13,13) element of Φ, and since most of Q is fixed to zero, the new estimates of Q are the (1,1), (2,2), and (13,13) elements of the above matrix, with all other elements set to zero. Here R is a scalar. The complete algorithm then consists of

1. Choose initial values for $x(0)$, Σ, and Θ.
2. Calculate the Kalman filter and smoother for the given parameter values.
3. Update the parameters by equation A12.
4. Iterate until convergence.

The Kalman smoothers, calculated at the final parameter estimates, produce the component time series.

Acknowledgments. The authors are grateful to Scott Woodruff (NOAA ERL) and Steve Worley (NCAR) for their assistance in securing the COADS data and Claude Roy for his efforts in preparing the data set. Richard Parrish is acknowledged for his scientific input and collaboration. We also thank Ted Strub, Robert Shumway, and three anonymous reviewers for their careful and constructive comments that greatly improved the manuscript.

References

Akaike, H., Likelihood and the Bayes procedure, in *Bayesian Statistics*, edited by J. M. Bernardo, M. H. DeGroot, D. V. Lindley and A. F. M. Smith, pp. 143-166, Univ. Press, Valencia, Spain, 1980.

Ansley, C. F., and R. Kohn, Estimation, filtering and smoothing in state space models with incompletely specified initial conditions, *Ann. Stat. 13*, 1286-1316, 1985.

Ansley, C. F., and R. Kohn, On the equivalence of two stochastic approaches to spline smoothing, in *Time Series and Allied Processes*, edited by J. Gani and M. B. Priestly, *J. Appl. Prob., 23A*, 391-405, 1986.

Ansley, C. F., and R. Kohn, Filtering and smoothing in state space models with partially diffuse initial conditions, *J. Time Ser. Anal., 11*, 275-293, 1990.

Bakun, A., Global climate change and intensification of coastal ocean upwelling, *Science, 247*, 198-201, 1990.

Bakun, A., Global greenhouse effects, multi-decadal wind trends, and potential impacts on coastal pelagic fish populations, *ICES Mar. Sci. Symp., 195*, 316-325, 1992.

Bakun, A., and C. S. Nelson, Climatology of upwelling related processes off Baja California, *Calif. Coop. Oceanic Fish. Invest. Rep., 19*, 107-127, 1977.

Bakun, A., and C. S. Nelson, The seasonal cycle of wind-stress curl in subtropical eastern boundary current regions, *J. Phys. Oceanogr., 21*, 1815-1834, 1991.

Brink, K. H., D. C. Chapman, and G. R. Halliwell Jr., A stochastic model for wind-driven currents over the continental shelf, *J. Geophys. Res., 92*, 1783-1797, 1987.

Brotherton, T., and W. Gersch, A data analytic approach to the smoothing problem and some of its variation, *Proc. IEEE Conf. Decision Contr., 20th,*, 1061-1069, 1981.

Cardone, V. J., J. G. Greenwood and M. Can, On trends in the historical marine wind data, *J. Clim., 3*, 113-127, 1990.

Cayan, D. R., Latent and sensible heat flux anomalies over the northern oceans: Driving the sea surface temperature, *J. Phys. Oceanogr., 22*, 859-881, 1992.

Cayan, D. R., D. R. McLain, W. D. Nichols, and J. S. DiLeo-Stevens, *Monthly climatic time series data from the Pacific Ocean and western Americas*, U.S. Geol. Surv. Open File Rep. 91-92, 379 pp., 1988.

Cury, P., and C. Roy, Optimal environmental window and pelagic fish recruitment success in upwelling areas, *Can. J. Fish. Aquat. Sci., 46*, 670-680, 1989.

De Jong, P., Smoothing and interpolation with the state-space model, *J. Am. Stat. Assoc., 84*, 1085-1088, 1989.

De Jong, P., Stable algorithms for the state space model, *J. Time Ser. Anal., 12*, 143-157, 1990.

De Jong, P., The diffuse Kalman filter, *Ann. Stat., 19*, 1073-1083, 1991.

Dempster, A. P., N. M. Laird, and D. B. Rubin, Maximum likelihood from incomplete data via the EM algorithm, *J. R. Stat. Soc., Ser. B., 39*, 1-38, 1977.

Denbo, D. W., and J. S. Allen, Large-scale response to atmospheric forcing of shelf currents and coastal sea level off the west coast of North America: May-July 1981 and 1982, *J. Geophys. Res., 92*, 1757-1782, 1987.

Dorman, C. E. and C. D. Winant, Buoy observations of the atmosphere along the west coast of the United States, 1981-1990. *J. Geophys. Res. 100*, 16,029-16,044, 1995.

Graham, N. E., Decadal scale variability in the 1970's and 1980's: Observations and model results, *Clim. Dyn., 10*, 60-70, 1994.

Harvey, A. C., *Forecasting, Structural Time Series Models and the Kalman Filter*, 554 pp., Cambridge Univ. Press, New York, 1989.

Hickey, B. M., The California Current System–Hypotheses and facts, *Progr. Oceanogr. 8*, 191-279, 1979.

Huyer, A., Coastal upwelling in the California Current System, *Progr. Oceanogr., 12*, 259-284, 1983.

Isemer, H.-J., Comparison of estimated and measured marine surface wind speed, in *Proc. Int. COADS Workshop, Boulder, Colorado, 13-15 January 1992*, edited by H. F. Diaz, K. Wolter, and S. D. Woodruff, pp. 142-158, U.S. Dep. of Commer., Washington, D.C., 1992.

Kitagawa, G., and W. Gersch, A smoothness priors - state space modeling of time series with trend and seasonality, *J. Am. Stat. Assoc., 79*, 378-389, 1984.

Kitagawa, G., and W. Gersch, A smoothness priors time varying AR coefficient modeling of nonstationary time series, *IEEE Trans. Autom. Control, AC-30*, 48-56, 1985.

Kitagawa, G., and W. Gersch, Smoothness priors in time series, in *Bayesian Analysis of Time Series and Dynamic Models*, edited by J. Spall, pp. 431-476, Marcel Dekker, New York, 1988.

Kohn, R., and C. F. Ansley, A new algorithm for spline smoothing and interpolation based on smoothing a stochastic process, *SIAM J. Sci. Stat. Comput., 8*, 33-48, 1987.

Kohn, R., and C. F. Ansley, The equivalence between Bayesian smoothness priors and optimal smoothing for function

estimation, in *Bayesian Analysis of Time Series and Dynamic Models*, edited by J. Spall, pp. 393-430, Marcel Dekker, New York, 1988.

Latif, M., and T. P. Barnett, Causes of decadal climatic variability over the North Pacific and North America, *Science, 266*, 634-637, 1994.

Lauritzen, S. L., Time series analysis in 1880: A discussion of contributions made by T. N. Thiele, *Int. Stat. Rev., 49*, 319-331, 1981.

Mann, M. E., and J. Park, Spatial correlations of interdecadal variation in global surface temperatures, *Geophys. Res. Lett., 20*, 1055-1058, 1993.

Mann, M. E., and J. Park, Global-scale models of surface temperature variability on interannual to century timescales, *J. Geophys. Res., 99*, 25,819-25,833, 1994.

Mann, M. E., and J. Park, Greenhouse warming and changes in the seasonal cycle of temperature: Model versus observations, *Geophys. Res. Lett., 23*, 1111-1114, 1996.

Mendelssohn, R., and C. Roy, Comprehensive ocean data extraction users guide, U.S. Dep. of Commer., *NOAA Tech. Memo. NOAA-TM-NMFS-SWFSC-228*, 67 pp., La Jolla, Calif., 1996.

Miller, A. J., D. R. Cayan, T. P. Barnett, N. E. Graham, and J. M. Oberhuber, Interdecadal variability of the Pacific Ocean: Model response to observed heat flux and wind stress anomalies, *Clim. Dyn., 9*, 287-302, 1994.

Parrish, R. H., C. S. Nelson, and A. Bakun, Transport mechanisms and reproductive success of fishes in the California Current, *Biol. Oceanogr., 1*, 175-203, 1981.

Parrish, R. H., A. Bakun, D. M. Husby, and C. S. Nelson, Comparative climatology of selected environmental processes in relation to eastern boundary current fish production, *FAO Fish. Rep., 291*, 731-778, 1983.

Rajagopalan, B., and U. Lall, Seasonality of precipitation along a meridian in the western United States, *Geophys. Res. Lett., 22*, 1081, 1995.

Roemmich, D., Ocean warming and sea level rise along the southwest U.S. coast, *Science, 257*, 373-375, 1992.

Roemmich, D., and J. McGowan, Climatic warming and the decline of zooplankton in the California Current, *Science, 267*, 1324-1326, 1995.

Rosenfeld, L. K., F. B. Schwing, N. Garfield, and D. E. Tracy, Bifurcated flow from an upwelling center: A cold water source for Monterey Bay, *Cont. Shelf Res., 14*, 931-964, 1994.

Sakuma, K. M., H. A. Parker, S. Ralston, F. B. Schwing, D. M. Husby and E. M. Armstrong, The physical oceanography off the central California coast during February-March and May-June, 1992: a summary of CTD data from pelagic young-of-the-year rockfish surveys, U.S. Dep. of Commer., *NOAA Tech. Memo. NOAA-TM-NMFS-SWFSC-208*, 169 pp., La Jolla, Calif., 1994.

Schwing, F. B., Long-term and seasonal patterns in coastal temperature and salinity along the North American west coast, in *Proc. Tenth Annual Pacific Climate (PACLIM) Workshop, Tech. Rep. 36*, edited by K. T. Redmond and V. L. Tharp, pp. 129-143, Interagency Ecol. Stud. Program for the Sacramento-San Joaquin Estuary, 1994.

Schwing, F. B., D. M. Husby, N. Garfield, and D. E. Tracy, Mesoscale oceanic response to wind events off central California in spring 1989: CTD surveys and AVHRR imagery, *Calif. Coop. Oceanic Fish. Invest. Rep., 32*, 47-62, 1991.

Schwing, F. B., R. Mendelssohn, and R. H. Parrish, Recent trends in the spatial structure of wind forcing and SST in the California Current System, in *Global Versus Local Changes in Upwelling Systems: Proc. 1st Int. CEOS Workshop*, edited by M.H. Durand, R. Mendelssohn, P. Cury, C. Roy and D. Pauly, ORSTOM, Paris, France, in press, 1997.

Shiller, R., A distributed lag estimator derived from smoothness priors, *Econometrica, 41*, 775-778, 1973.

Shumway, R. H., *Applied Statistical Time Series Analysis*, 379 pp., Prentice-Hall, Englewood Cliffs, N.J., 1988.

Shumway, R. H., and D. S. Stoffer, An approach to time series smoothing and forecasting using the EM algorithm, *J. Time Ser. Anal., 3*, 253-264, 1982.

Slutz, R. J., S. J. Lubker, J. D. Hiscox, S. D. Woodruff, R. L. Jenne, D. H. Joseph, P. M. Steurer, and J. D. Elms, *Comprehensive Ocean-Atmosphere Data Set; Release 1*, 268 pp., NOAA Environ. Res. Lab., Clim. Res. Program, Boulder, Colo., 1985.

Strub, P. T., J. S. Allen, A. Huyer, R. L. Smith, and R. C. Beardsley, Seasonal cycles of currents, temperature, winds, and sea level over the northeast Pacific continental shelf: 35°N to 48°N, *J. Geophys. Res., 92*, 1507-1526, 1987.

Thiele, T. N., Om Anvedelse af Mindste Kvadraters Methode i Nogle Tilfaelde, hvor en Komlikation af visse Slags uensartede tilfaeldige Fejlkilder giver Fejlene en "systematisk" Karakter, *Vidensk. Selsk. Skr., Naturvid Mat. Afd., 12*, 381-408, 1880.)

Thomson, D. J., The seasons, global temperature, and precession, *Science, 268*, 59, 1995.

Trenberth, K. E, Recent observed interdecadal climate changes in the northern hemisphere, *Bull. Am. Meteorol. Soc., 71*, 988-993, 1990.

Trenberth, K. E., and J. W. Hurrell, Decadal atmospheric-ocean variations in the Pacific, *Clim. Dyn., 9*, 303-319, 1994.

Wahba, G., *Spline Functions for Observational Data, CBMS-NSF Regional Conf. Ser. in Appl. Math.*, vol. 59, SIAM, Philadelphia, Pa., 1990.

Ware, D. M., A century and a half change in the climate of the NE Pacific, *Fish. Oceanogr., 4*, 267-277, 1995.

Walker, P. M., D. M. Newton, and A. W. Mantyla, Surface water temperatures, salinities and densities at shore stations, United States West Coast, 1992, *SIO Ref. 93-18*, 46 pp., Univ. of Calif., San Diego, Scripps Inst. of Oceanog., La Jolla, Calif., 1993.

Wecker, W. E., and C. R. Ansley, The signal extraction approach to nonlinear regression and spline smoothing, *J. Am. Stat. Assoc., 78*, 81-89, 1983.

Whittaker, E. T., On a new method of graduation, *Proc. Edinborough Math. Assoc., 78*, 81-89, 1923.

Woodruff, S. D., R. J. Slutz, R. L. Jenne, and P. M. Steurer, A comprehensive ocean-atmosphere data set, *Bull. Am. Meteorol. Soc., 68*, 1239-1250, 1987.

Wu, Z., and R. E. Newell, The wind problem in COADS and its influence on the water balance, in *Proc. Int. COADS Workshop, Boulder, Colorado, 13-15 January 1992*, edited by H. F. Diaz, K. Wolter and S. D. Woodruff, pp. 189-200, U.S. Dep. of Commer., Washington, D.C., 1992.

Xie, L., and W. W. Hsieh, The global distribution of wind-induced upwelling, *Fish. Oceanogr., 4*, 52-67, 1995.

Young, P. C., C. N. Ng, K. Lane, and D. Parker, Recursive forecasting, smoothing and seasonal adjustment of non-stationary environmental data, *J. Forecasting, 10*, 57-89, 1991.

R. Mendelssohn and F. B. Schwing, NOAA-NMFS, Southwest Fisheries Science Center, Pacific Fisheries Environmental Group, 1352 Lighthouse Avenue, Pacific Grove, CA 93950. (e-mail: rmendels@pfeg.noaa.gov; fschwing@pfeg.noaa.gov)

(Received July 31, 1995; revised October 16, 1996; accepted October 22, 1996.)